Available online at www.sciencedirect.com

ScienceDirect

Procedia CIRP 94 (2020) 742–747

www.elsevier.com/locate/procedia

11th CIRP Conference on Photonic Technologies [LANE 2020] on September 7-10, 2020

Correlation analysis between the beam propagation and the vapor capillary geometry by machine learning

Christian Stadter[a,*], Michael K. Kick[a], Maximilian Schmoeller[a], Michael F. Zaeh[a]

[a]*Institute for Machine Tools and Industrial Management (iwb), Technical University of Munich, Boltzmannstrasse 15, 85748 Garching, Germany*

* Corresponding author. Tel.: +49-89-289-15560; fax: +49-89-289-15555. *E-mail address:* christian.stadter@iwb.tum.de

Abstract

Low Coherence Interferometry allows for a direct inline measurement of the capillary depth during laser material processing. To enable a robust interpretation of the measurement results, a large number of influencing factors have to be considered. The geometry of the vapor capillary significantly affects the reflection behavior of the measuring radiation. Particularly, with capillary dimensions in the order of the magnitude of the measuring beam, scattering and absorption effects become significant. This paper describes the utilization of a ray tracing algorithm to analyze the beam propagation within the capillary. A keyhole generator and Machine Learning methods were applied for systematic investigations of the propagation of the measuring radiation and thus enabled an improved interpretation of capillary depth measurements.

Keywords: Ray tracing; Weld depth measurement; Laser material processing; Process data interpretation; Machine Learning

1. Introduction

The highly dynamic and highly focused deposition of energy during laser beam welding results, on the one hand, in the process-inherent advantages compared to other joining technologies, but, on the other hand, also in the major challenges for an industrial deployment of this technology. The high process dynamics and their effect on the product quality require a real-time assessment of critical process factors. Low Coherence Interferometry allows for the in-situ measurement of optical path lengths coaxially to the processing laser beam. As process emissions have hardly any influence on the interferometric principle [1], the high-precision and temporally high-resolution measurement of the capillary depth contains a multitude of process-related influences and effects without significant disturbances [2]. Ray tracing allows for a geometrical representation of the beam propagation within the vapor capillary and by analyzing those an improved interpretation of in-situ weld depth measurements.

2. Low Coherence Interferometry

Optical Coherence Tomography (OCT) as one method of Low Coherence Interferometry has been established as a high-precision measuring technique since 1972. Utilizing the principles proposed by A. A. MICHELSON and a broadband light source, OCT allows absolute distances to be evaluated based on interferometric measurements [3]. One reason for the broad establishment of this technology is the robust evaluation of the interference patterns, which can already be reliably performed with reflected light fractions of 10^{-10} of the initial measuring beam [4]. By evaluating the interference in the frequency rather than in the time domain, the acquisition time for topographic scans could be reduced drastically [5], whereas the sensitivity could be enhanced even further [6]. This made high-precision measurements with a temporal resolution of several hundred kilohertz [7] possible even in the presence of process emissions, such as they are present during laser beam welding [8].

10.1016/j.procir.2020.09.138

Figure 1 illustrates the measuring principle of FOURIER Domain OCT. As the setup is free of moving parts, the acquisition rate is only limited by the sampling rate of the detector array that is used to analyze the interference between the measuring and the reference beam.

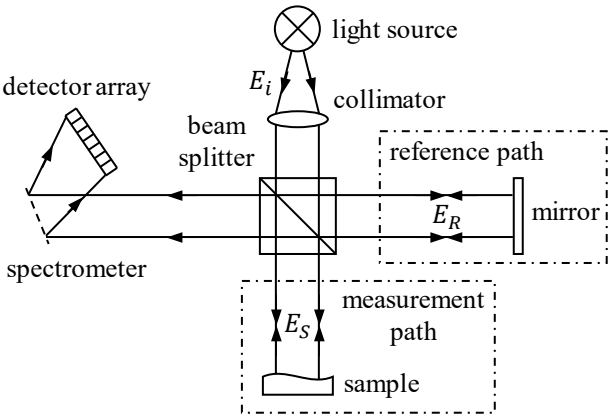

Fig. 1. Measuring principle of FOURIER Domain OCT (based on [9]).

Assuming an equal and wavelength-independent split of the measuring light into the reference and the measuring beam, the polychromatic illumination with the complex electric field

$$E_i = s(k,\omega)e^{i(kz-\omega t)} \tag{1}$$

determines the electric fields in the measurement and the reference path [10]:

$$E_R = \frac{E_i}{\sqrt{2}} r_R e^{i2kz_R},\ E_S = \frac{E_i}{\sqrt{2}} \sum_{n=1}^{N} r_{Sn} e^{i2kz_{Sn}} \tag{2}$$

Here, s is the amplitude of the electric field as a function of the wave number k and the angular frequency ω, z is the coordinate in the direction of the beam propagation and t is the time. In general, multiple reflections n at the position z_{Sn} and the respective power reflectivity $R_{Sn} = |r_{Sn}|^2$ are included. This can be used to calculate the photo current in the detector I_D as a result from the superposition of the electric fields E_R and E_S [10]:

$$I_D(k,\omega) = \frac{\rho}{2}\langle |E_R + E_S|^2 \rangle \tag{3}$$

Equation 3 includes the responsivity of the sensor ρ and the time average $\langle\cdot\rangle$, i.e. the integration over the response time [7]:

$$\langle f \rangle = \lim_{T\to\infty} \frac{1}{2T} \int_{-T}^{T} f(t)dt \tag{4}$$

Thus, the temporally invariant terms of the detector current can be assessed according to equation 5 [10]. The spectral power as a function of the wave number $S(k)$ can be simplified for assuming a GAUSSIAN shaped spectrum which is typically applicable for light sources used in FD OCT [10]:

$$\begin{aligned} I_D(k) &= \frac{\rho}{4}[S(k)(R_R + R_{S1} + R_{S2} + \ldots)] \\ &+ \frac{\rho}{4}\left[S(k)\sum_{n=1}^{N}\sqrt{R_R R_{Sn}}\left(e^{i2k(z_R - z_{Sn})} + e^{-i2k(z_R - z_{Sn})}\right)\right] \\ &+ \frac{\rho}{4}\left[S(k)\sum_{n\neq m=1}^{N}\sqrt{R_{Sn}R_{Sm}}\left(e^{i2k(z_{Sn} - z_{Sm})}\right.\right. \\ &\left.\left. + e^{-i2k(z_{Sn} - z_{Sm})}\right)\right] \end{aligned} \tag{5}$$

With the central wave number k and the bandwidth of the light source spectrum Δk, the spectral power becomes [10]

$$S(k) = \langle |s(k,\omega)|^2 \rangle = \frac{1}{\Delta k\sqrt{\pi}} e^{-\left[\frac{k-k_0}{\Delta k}\right]^2} \tag{6}$$

To calculate the distance to the object to be measured z_S, the term $\sqrt{R_S(z_S)}$ can be specified as the sum $\sum_{n=1}^{N}\sqrt{R_{Sn}}\delta(z_S - z_{Sn})$ resulting from N discrete reflections. The distance z_S can be determined by an inverse FOURIER transformation [10], for which suitable simplifications and relevant parameters for various spectral characteristics of the setup can be found in [11]. Figure 2 illustrates an exemplary raw detector signal considering two reflections in the measurement path and the corresponding signal after an inverse FOURIER transformation.

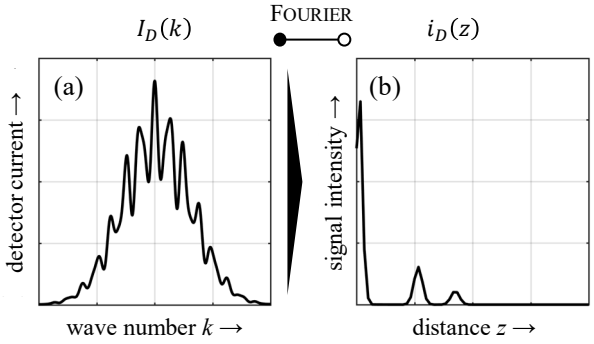

Fig. 2. (a) Raw detector signal as a function of the wave number; (b) FOURIER transformed signal in FD OCT (based on [9]).

3. State of the art

Due to the non-contact measuring principle and the high precision, optical systems have been established in laser material machining in general [12] and proven to be advantageous especially in laser beam welding for monitoring and controlling purposes [13]. The following review therefore focuses on OCT as the only optical method that allows dimensional in-situ measurements and on methods for analyzing the measuring beam propagation.

3.1. Inline weld depth measurement

DE BONO ET AL. demonstrated the applicability of OCT to coaxially measure the capillary depth during laser beam welding using a fixed optics setup. Based on reference trials and metallographic cross sections, it was demonstrated that the

measuring system allows the welding depth to be determined during partial penetration welding. [14]

KOGEL-HOLLACHER ET AL. discussed the capability of OCT to capture surface height profiles. The measuring and the processing laser beam were deflected coaxially by means of a scanning device. The setup facilitated in-situ recordings of the surface topography during processing with ultra-short laser pulses. [1]

WEBSTER ET AL. developed an OCT system to measure the machining depth during remote laser processing. Based on the monitoring of the ablation depth, an automatic sculpting of 3D structures could be performed [15]. Supplemented with a closed-loop feedback control, the machining depth could be resolved with up to 230 kHz and a depth resolution of about 7 µm [16].

SCHMOELLER ET AL. investigated OCT-based measurements of the weld depth using high-brilliance laser radiation. The effect of the material, the weld depth and the angle of incidence on the capillary depth signal were quantified by statistical measures. It was demonstrated that OCT can be applied for weld depth measurements with single-mode radiation and spot sizes down to 55 µm [2]. Further investigations in the pre- and post-process zone assessed the possibilities regarding inline process control and quality assurance purposes. Fundamental influencing factors on the OCT measurement were identified and the resulting accuracy was specified [17].

3.2. Beam propagation analysis for laser beam welding

The propagation of light can be precisely described by solving the MAXWELL's equations for electromagnetic waves. The consideration of the wave nature and its effects on the propagation of light, however, is accompanied by high computational efforts. For applications where a purely geometrical consideration of the beam propagation provides sufficient accuracies, ray tracing algorithms become advantageous.

BERGSTROEM developed a 2D and a 3D ray tracing algorithm to investigate the absorptivity of metal surfaces for laser radiation. As part of the simulative approach, a method to create random surfaces with a GAUSSIAN distributed surface roughness was developed. It could be observed that a noticeable increase in the absorptivity occurs for a surface roughness above a specific threshold due to multiple reflections within the surface cavities. [18]

COURTOIS ET AL. described the propagation of electromagnetic waves based on the stationary MAXWELL's equations and a computational fluid dynamics model. A 2D axial-symmetric model was created to analyze the keyhole formation and the following solidification in deep penetration welding processes. Process specific failures such as the generation of pores and melt pool instabilities could be analyzed numerically. [19]

GANSER ET AL. presented a method to efficiently determine the reflections during deep penetration welding on the entire hemisphere around the process zone. A theoretical model was combined with a radiation analyzer, that was utilized to calibrate the model by measurements at selected reference points. [20]

HORNÍK ET AL. analyzed the back reflections during deep penetration laser beam welding. The back-reflected radiation was measured and correlated to the depth and the width of the weld seams. A mathematical model using ray tracing was developed to describe the propagation of the back reflections based on the assumption of an inclined conical cavity representing the capillary that is formed during deep penetration welding. [21]

4. Objectives and approach

Due to the process-immanent challenges, the monitoring of laser beam welding has been the focus of intensive research for decades. OCT provides, for the first time, the possibility of an in-situ recording of direct process parameters during laser beam welding [22]. To evaluate the high-resolution data, which are superimposed with a multitude of complex and dynamic process phenomena, Machine Learning methods have proven to be a powerful tool [23]. The capillary geometry is decisive for a significant share of the quality-determining effects during welding and the majority of the mechanical properties of the weld seam.

Fundamental investigations were thus performed to identify correlations between the signal structure of inline weld depth measurements and the capillary geometry. Artificial Neural Networks and Gaussian Process Regression models were deployed to predict the capillary geometry based on the inline process data, cf. Figure 3. A ray tracing algorithm was utilized to systematically analyze the beam propagation of the measuring radiation depending on the capillary geometry.

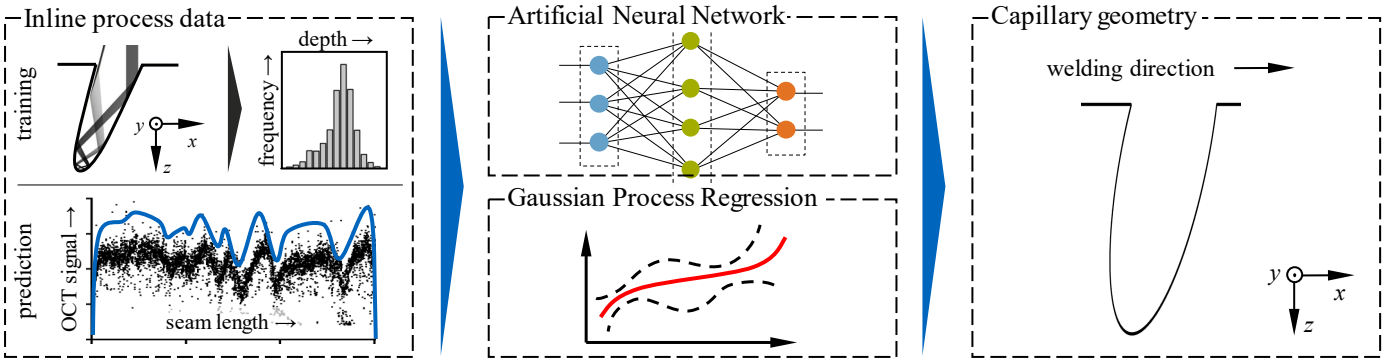

Fig. 3. Prediction of the capillary geometry based on inline weld depth measurements using Artificial Neural Networks and Gaussian Process Regression models.

5. Numerical and supervised learning model approach

To predict the keyhole geometry based on inline weld depth measurements, a profound understanding of the relationship between the measuring beam propagation and the capillary geometry is required. For this reason, based on an automated generation of capillary geometries, the beam propagation was calculated by means of a ray tracing algorithm. With the obtained information about the distance covered by each measuring beam, a supervised Machine Leaning model was trained to predict the capillary geometry. Its components and the procedure are shown in Fig. 4 and described in detail below.

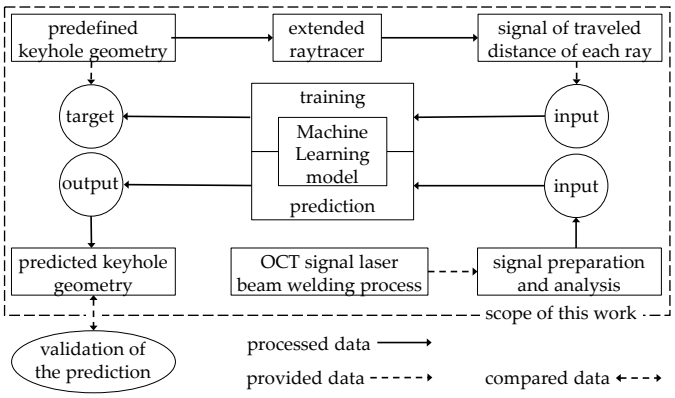

Fig. 4. Components and procedure to predict the keyhole geometry.

5.1. Ray tracing

A module for the automatic generation of keyhole geometries that represent the vapor capillary during welding was developed to systematically assess the effect of the geometry on the beam propagation. The capillary was generated and parameterized based on geometries that are usually observed during welding, as they are exemplarily shown in [24]. Process-specific as well as geometry-specific parameters were considered to represent the target geometries as shown exemplarily in Fig. 5.

Besides the capillary depth, the angle of incidence, the opening diameter and its center position as process-specific parameters, the geometry-specific parameters of the implemented shapes are provided in Table 1.

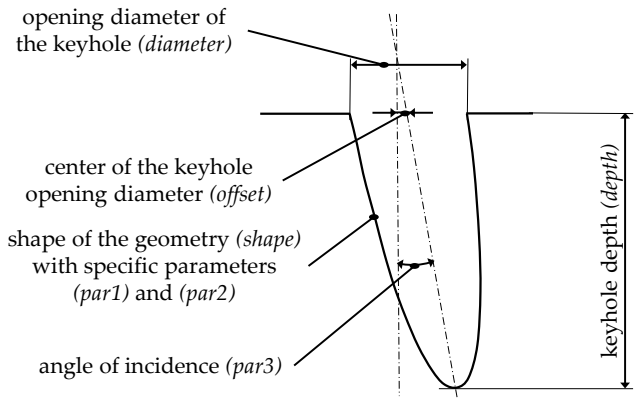

Fig. 5. Parameters considered for the automated keyhole generation.

Table 1. Implemented shapes in the keyhole generator.

shape	shape parameter *par1*	shape parameter *par2*
sphere	diameter of the sphere	–
ellipsis	semi-minor axis	semi-major axis
cone	radius of the cone	–
cylinder	diameter of the cylinder	inclination of the bottom

A 2D ray tracing approach was used to calculate the beam propagation. Based on the method of BERGSTROEM [18], a ray tracer capable of considering undercuts was developed. To calculate the beam propagation, the beam characteristics of the measuring radiation were included and the length of each simulated ray was measured during its propagation within the capillary. The detailed characteristics of the measurement beam are listed in [23].

5.2. Neural Network and Gaussian Process Regression

The basis for the supervised learning approach is the specification of the input and the target data. The input was defined by the traveled distance of each ray (cf. Fig. 4). The target was created based on the image representation of the corresponding capillary geometries. The representation of the geometry allows a significant reduction in the dimensionality without losing information about the shape. Fig. 6 illustrates that for each column of the image there are only a maximum of 3 intersections with the capillary shape and only these have to be considered as coordinates to completely reproduce the geometry. The coordinates of the intersections of each column were then assigned to the target vector $\boldsymbol{y}$.

Compared to the commonly used procedure of training separate models for each pixel [25], a significant reduction in complexity could be achieved with this approach with increasing image resolutions. A data set consisting of 35 elliptic keyholes was used for the supervised learning. The data were mapped to values from -1 to +1, randomized and split into 27 geometries for the training and 8 for the testing. Keyhole depths ranging from 1 to 4 mm, angles of incidence between +10° (dragging process) and -15° and opening diameters between 50 µm and 300 µm were considered. The feedforward Artificial Neural Network was built from one hidden layer, using a tangent hyperbolic function for the activation in the hidden layer and a linear function for the output activation. Scaled conjugate gradient backpropagation was applied for the training process. In addition, a nonparametric kernel-based probabilistic model based on Gaussian Process Regression was utilized.

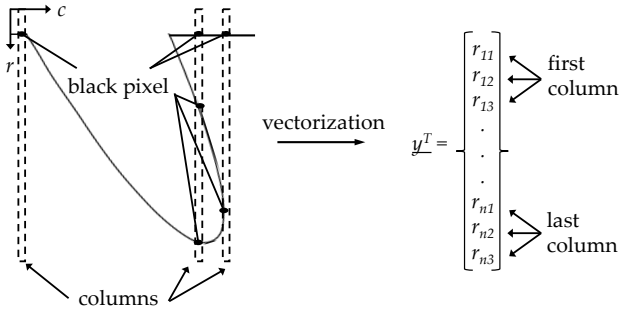

Fig. 6. Procedure to create the target $\boldsymbol{y}$ based on the keyhole geometry.

6. Results and discussion

The basis for evaluating the ray tracing approach was formed by the results of experimental weld depth measurements carried out by means of OCT and validated by metallographic cross-sections on the aluminum alloy AA6082. The typical signal characteristics are shown in Fig. 7. The distinct variance of the measured capillary depths was characterized by the relative frequency distribution of the measuring samples. Even in areas without macroscopic fluctuations of the welding depth, as they can be seen in Fig. 7 (b), the challenge to determine the actual depth from the scattered point cloud is evident.

Experimental investigations showed a strong dependence of the signal variance as well as the deviation of the measured depths from the actual welding depth depending on the angle of incidence and the welding depth [2]. Therefore, the effects of the capillary depth and the angle of incidence relative to the laser beam axis on the beam propagation were investigated. The distributions of the measured lengths of the simulated measuring beams are given in Fig. 8. A representative capillary geometry was selected and parameterized for the analyses. Based on findings from simulation studies on laser beam welding [26, 27], an elliptical shape with an opening diameter of 175 µm and a vertical orientation ($\alpha = 0°$) were chosen.

With increasing depths, a decrease of the relative frequency, which corresponds to the set keyhole depth $t_{KH,set}$ and results from a direct reflection at the bottom of the cavity, could be observed. The relative frequency of shorter path lengths increased significantly, which can be attributed to reflections at the capillary walls. This is in good agreement with observations from measurements, in which a significant decrease in the proportion of measurements presumably resulting from reflections at the capillary bottom was observed [2]. This was found to be particularly relevant for high aspect ratios resulting from highly brilliant radiation [2].

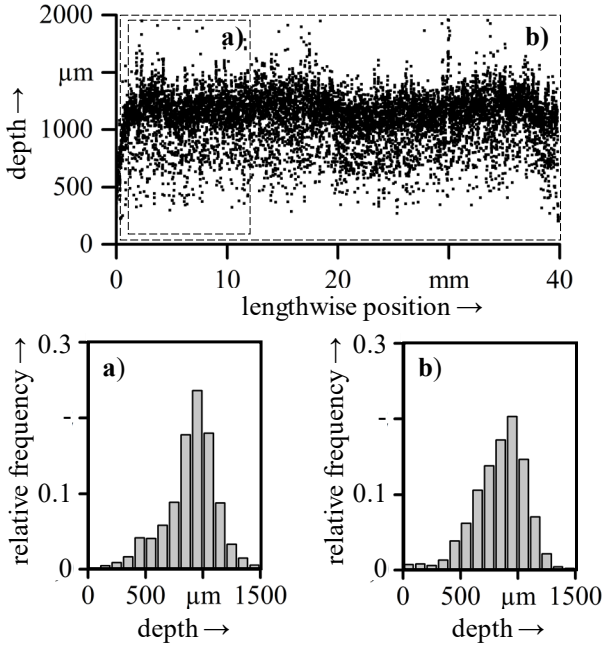

Fig. 7. Relative frequency distribution of measured weld depths for AA6082 along the entire weld seam (a) and within a stable process regime (b) [2].

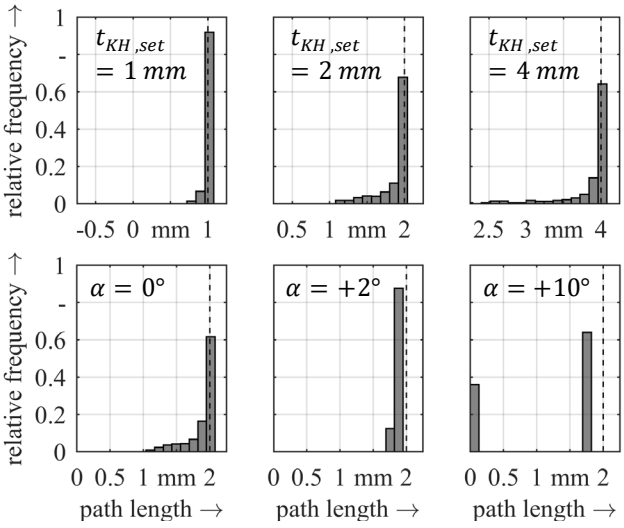

Fig. 8. Probability density function of the path length of the simulated rays depending on the keyhole depth (above) and the angle of incidence (below).

For an inclination of the capillary, a contrary effect was found at medium deflections. With increasing angles, a decline of reflections from the capillary was detected. This behavior was observed for both positive (dragging) and negative (piercing) angles of incidence. Also, a shift of the highest probability density towards shorter lengths with increasing inclination angles could be noticed. A strong dependence of the variance of depth values on the angle of incidence was also observed in experiments [2]. To clarify the underlying causes, however, further investigations are necessary, as angles of incidence between -10° and +10° have not been systematically investigated experimentally due to strong back reflections.

Based on the data set consisting of 35 geometries, Artificial Neural Networks as well as Gaussian Process Regression models were trained. The lengths of 25 simulated rays were used as the input for the models. The vectorized coordinates were considered as the output (cf. Fig. 6). For visualization reasons, a component located in the middle of the geometry was chosen to evaluate the prediction. Fig. 9 shows the prediction accuracy measured as mean squared error (MSE) as a function of the number of neurons in the hidden layer. With deviations of $e_{MSE} \approx 0.2$, corresponding to geometrical deviations of about 10 %, decent prediction accuracies could be achieved.

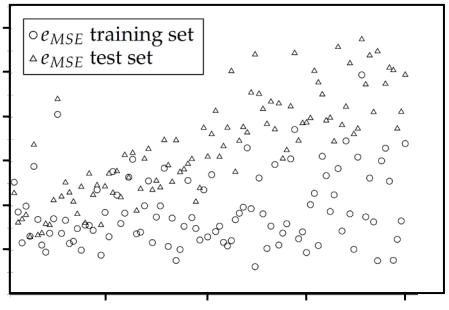

Fig. 9. Influence of the number of neurons on the prediction accuracy measured by the MSE for a Neural Network with one hidden layer.

For the models based on Gaussian Process Regression, a minimum error of $e_{MSE} \approx 0.4$ could be attained by varying the kernel function. As the matern function and the squared exponential function with a separate length scale per predictor did not lead to higher prediction accuracies, no further investigations were conducted with these models.

7. Summary and outlook

To enable a precise and reliable interpretation of inline weld depth measurements, a framework including the following components was elaborated:

- A keyhole generator for the automated creation and parametrization of capillary geometries
- A 2D ray tracing approach to calculate the beam propagation within complex cavities
- A Machine Learning method to predict the keyhole geometry based on the probability density of depth values

Analyses of simulated and measured courses of the capillary depth during welding yielded the following findings:

- A geometrical ray tracing approach can be exploited to clarify the dependence of the OCT signal characteristics on the angle of incidence and the welding depth.
- A data reduction strategy can be utilized to drastically cut the dimensionality of the geometrical specification of the capillary shape for supervised learning methods.
- Neural Networks can be deployed to predict the keyhole shape based on depth values and a data set of 35 capillary geometries with an accuracy of approximately 10 %.

Subsequent research will focus on the experimental validation and explore the validity limits of the keyhole geometry predictions based on measured data (cf. Fig. 4).

Acknowledgements

The results presented were achieved within the RoKtoLas project, which is supported by the German Federal Ministry of Education and Research (BMBF) within the Photonics Research Germany funding program (contract number 13N14555) and supervised by the VDI Technology Center (VDI TZ). We would like to thank the BMBF and the VDI TZ for their support and for the effective and trusting cooperation.

References

[1] Kogel-Hollacher, M., Schoenleber, M., Schulze, J., Pichot, J.F., 2017. Inline measurement for quality control from macro to micro laser applications. Laser Applications in Microelectronic and Optoelectronic Manufacturing (LAMOM) XXII. SPIE LASE, San Francisco, California, USA. 28 January 2017. SPIE.

[2] Schmoeller, M., Stadter, C., Liebl, S., Zaeh, M.F., 2019. Inline weld depth measurement for high brilliance laser beam sources using optical coherence tomography. Journal of Laser Applications 31 (2), p. 22409.

[3] Flournoy, P.A., McClure, R.W., Wyntjes, G., 1972. White-light interferometric thickness gauge. Applied optics 11 (9), pp. 1907–1915.

[4] Huang, D., Swanson, E., Lin, C., Schuman, J., Stinson, W., Chang, W., Hee, M., Flotte, T., Gregory, K., Puliafito, C., 1991. Optical coherence tomography. Science 254 (5035), pp. 1178–1181.

[5] Chinn, S.R., Swanson, E.A., Fujimoto, J.G., 1997. Optical coherence tomography using a frequency-tunable optical source. Optics Letters 22 (5), p. 340.

[6] Boer, J.F. de, Cense, B., Park, B.H., Pierce, M.C., Tearney, G.J., Bouma, B.E., 2003. Improved signal-to-noise ratio in spectral-domain compared with time-domain optical coherence tomography. Optics Letters 28 (21), p. 2067.

[7] Bernardes, R., Cunha-Vaz, J., 2012. Optical coherence tomography: A clinical and technical update. Springer, Heidelberg, xv, p. 255.

[8] Fraser, J.M., 2012. Laser process monitoring and automatic control at kHz rates through inline coherent imaging. International Symposium on High Power Laser Ablation, New Mexico, USA. 30.04.-03.05.2012. American Institute of Physics, pp. 492–496.

[9] Donges, A., Noll, R., 2015. Laser Measurement Technology: Fundamentals and Applications. Springer, Heidelberg, p. 18.

[10] Drexler, W., 2008. Optical coherence tomography: Technology and applications. Springer, Berlin, p. 1346.

[11] Tomlins, P.H., Wang, R.K., 2005. Theory, developments and applications of optical coherence tomography. J. Phys. D: Appl. Phys. 38 (15), pp. 2519–2535.

[12] Purtonen, T., Kalliosaari, A., Salminen, A., 2014. Monitoring and Adaptive Control of Laser Processes. Physics Procedia 56, pp. 1218–1231.

[13] Lee, S.K., Na, S.J., 2002. A study on automatic seam tracking in pulsed laser edge welding by using a vision sensor without an auxiliary light source. Journal of Manufacturing Systems 21 (6), p. 489.

[14] Bono, P., Allen, C., D'Angelo, G., Cisi, A., 2017. Investigation of optical sensor approaches for real-time monitoring during fibre laser welding. Journal of Laser Applications 29 (2), p. 22417.

[15] Webster, P.J.L., Wright, L.G., Ji, Y., Galbraith, C.M., Kinross, A.W., van Vlack, C., Fraser, J.M., 2014. Automatic laser welding and milling with in situ inline coherent imaging. Optics Letters 39 (21), pp. 6217–6220.

[16] Ji, Y., Grindal, A.W., Webster, P.J.L., Fraser, J.M., 2015. Real-time depth monitoring and control of laser machining through scanning beam delivery system. J. Phys. D: Appl. Phys. 48 (15), p. 155301.

[17] Stadter, C., Schmoeller, M., Zeitler, M., Tueretkan, V., Munzert, U., Zaeh, M.F., 2019. Process control and quality assurance in remote laser beam welding by optical coherence tomography. Journal of Laser Applications 31 (2), p. 22408.

[18] Bergström, D., 2008. The Absorption of Laser Light by Rough Metal Surfaces, p. 226.

[19] Courtois, M., Carin, M., Le Masson, P., Gaied, S., Balabane, M., 2013. A new approach to compute multi-reflections of laser beam in a keyhole for heat transfer and fluid flow modelling in laser welding. J. Phys. D: Appl. Phys. 46 (50), p. 505305.

[20] Ganser, A., Liebl, S., Schmitz, P., Zaeh, M.F., 2016. Detection of transient reflections during laser beam welding of copper. SPIE LASE, San Francisco, California, USA. 13.02.2016. SPIE, 97410.

[21] Horník, P., Šarbort, M., Šebestová, H., Mrňa, L., 2019. Study of the influence of focal position on back-reflected radiation during deep penetration laser welding and its simulation. Optics and Measurement International Conference. Optics and Measurement International Conference, Liberec, Czech Republic. 08.10.–10.10.2019. SPIE, p. 11.

[22] Stadter, C., Schmoeller, M., Zeitler, M., Tueretkan, V., Munzert, U., Zaeh, M.F., 2019. Process control and quality assurance in remote laser beam welding by optical coherence tomography. Journal of Laser Applications 31 (2), p. 22408.

[23] Stadter, C., Schmoeller, M., Rhein, L. von, Zaeh, M.F., 2019. Real-time prediction of quality characteristics in laser beam welding using optical coherence tomography and machine learning. LIA (Ed.), Proceedings of the International Congress of Lasers & Electro-Optics (ICALEO).

[24] Steen, W.M., Mazumder, J., 2010. Laser Material Processing. Springer London, p. 567.

[25] Krutzlinger, M., Meltzer, E., Muehlegg, M., Zaeh, M.F., 2019. Gaussian process regression to predict the morphology of friction-stir-welded aluminum/copper lap joints. Int J Adv Manuf Technol 102 (5-8), pp. 1839–1852.

[26] Liebl, S., Stadter, C., Ganser, A., Zaeh, M.F., 2017. Numerical simulation of laser beam welding using an adapted intensity distribution. Journal of Laser Applications 29 (2), p. 22405.

[27] Schmoeller, M., Neureiter, M., Stadter, C., Zaeh, M.F., 2019. Numerical Weld Pool Simulation for the Accuracy Improvement of Inline Weld Depth Measurement Based on Optical Coherence Tomography. LIA (Ed.), Proceedings of the International Congress of Lasers & Electro-Optics (ICALEO).